Bioremoval mechanisms of azo dye Acid Red 14 using *Wickerhamomyces anomalus* yeast strain as a natural biosorbent

Mohammed Danouche (mohammed.danouche@usmba.ac.ma)
Moroccan Foundation for Advance Science Innovation and Research https://orcid.org/0000-0003-1654-8372
Hicham El Arroussi
MASCIR: Moroccan Foundation for Advance Science Innovation and Research
Naima El Ghachtouli
USMBA FSTF: Universite Sidi Mohamed Ben Abdellah Faculte des Sciences et Techniques de Fes

Research

Keywords: Wickerhamomyces anomalus, Azo dye, Biosorption, Isotherm and Kinetic model, Biomass characterization, Optimization

Posted Date: May 3rd, 2021

DOI: https://doi.org/10.21203/rs.3.rs-415931/v1

Abstract

Biosorption processes have recently become an economic and eco-friendly solution for the treatment of industrial wastewater. This study aimed to evaluate the potential application of *Wickerhamomyces anomalus* as a natural biosorbent for the removal of toxic synthetic dye Acid Red 14 (AR14). Biosorption kinetics modelling showed that the pseudo-second-order and intraparticle diffusion models were more suitable to fit the experimental data. In addition, the Langmuir model was the most appropriate isotherm to explain the AR14-*W. anomalus* biosorption system. Thus, the physicochemical properties of *W. anomalus* biomass before and after dye biosorption were characterized by scanning electron microscopy with energy dispersive X-Ray analysis, fourier-transform infrared spectroscopy, zeta potential, zero-point charge and contact angle measurement. The functional groups such as hydroxyl, carboxyl, amide, and amine present on the yeast wall surface can be responsible for AR14 biosorption. Finally, the Plackett-Burman design was used to screen the most influencing factors on the biosorption process, including dye concentration, dose of yeast biomass, temperature, shaking speed, and contact time. The latter was optimized according to the Box-Behnken design and the optimum AR14-biosorption was attained at pH 3–4, with lower initial dye concentrations (50–75 mg L^{-1}) and yeast biomass (1.25 g L^{-1}). These findings suggest that *W. anomalus* biomass could be used as an efficient, low-cost, and eco-friendly biosorbent for the removal of toxic dyes from the aqueous environment.

1. Introduction

Worldwide, the textile industry is one of the leading fast-growing businesses. However, for the production of 1 kg of finished textile products, this manufacturing process requires between 200–500 L of water, which makes this sector one of the largest producers of liquid effluents [1]. It has also been estimated that approximately 10 000 tons per year of synthetic dyes are used in this sector, of which 10–15% are rejected as waste during the dyeing process [2]. Unfortunately, the release of such toxic effluents into the environment does not only affect negatively the color of water, but results into serious toxicity impact to exposed species including humans [3]. To deal with this issue, strict regulations have been implemented to manage the release of such xenobiotics into the environment. Also, several approaches have been proposed as solutions for their treatment, such as membrane processes, photochemical oxidation processes, and electrochemical processes. Although these methods are effective, they require chemicals and energy-intensive equipment, which makes them expensive, thereby limiting their large-scale applications [4]. Recently, increasing attention has been focused on new effective, environmentally friendly, and low-cost technologies, such as adsorption techniques. Activated carbon is the most commonly used adsorbent material [5]. Nevertheless, thermal or chemical regeneration as well as the need for complexing agents to improve their performance, make the use of activated carbon-based processes expensive, and therefore limit their large-scale practical application [6]. New effective, readily available and low-cost adsorbents are on request in wastewater treatment plants. Hence, the use of biological materials (biosorbents) such as natural residues, industrial food wastes, agricultural wastes, and biomass of various microorganisms has been reported to be cheap and efficient alternatives [7]. In

fact, several studies have been reported the potential application of microalgae, cyanobacteria, and filamentous fungi in the biosorption of toxic dyes from wastewater [8–10]. However, only a few studies have focused on yeast cell, despite their advantages over other taxa, in particularly their fast growth compared to filamentous fungi or microalgae [11], their ability to survive in harsh environments [12], and their special flocculating characteristic that allows them to aggregate into multicellular masses (flakes), facilitating, therefore, their recovery after treatment of colored effluents [13]. Hence, with the aim to evaluate the potential application of *Wickerhamomyces anomalus* in the biosorption of Acid red 14 (AR14), the specific objectives of this research were: (i) to explain the biosorption mechanism and modeling the reactions involved in this process, (ii) to characterize the yeast biomass before and after dye biosorption, and (iii) to optimize the biosorption process using the design of experiment.

2. Material And Methods

2.1 Chemicals

The monoazo dye AR14 (1-Naphthalenesulfonic acid, 4-hydroxy-3-((4-sulfo-1-naphthalenyl) azo)-, disodium salt), commonly used in the textile, paper, food, etc. industries, was used in this study as a model pollutant. The dye solution was prepared at concentration of 5 $g.L^{-1}$ in distilled water, then sterilized by filtration and store at 4 ºC. All other chemicals used for this study were of analytical grade reagents, and were purchased from Sigma and Merck.

2.2 Yeast source, culture medium and biosorbent preparation

This study was conducted with the yeast strain of *W. anomalus*, previously isolated from a contaminated site located in Oued Sebou, Fez (Morocco). Its pure culture was maintained on Yeast Extract–Peptone–Glucose (YPG) medium (2% Difco peptone, 1% yeast extract and 2% glucose) [14]. Biosorbent preparation was carried out after 24 h of yeast growth, the biomass was recovered by centrifugation at 10 000xg for 10 min and the pellet was inactivated by autoclaving (121 ºC for 45 min). The regression equation of OD_{600nm} and the dry cell weight (DCW) was calculated on the basis of the standard curve according to Eq. (1).

$DCW = 0.2418 \times OD_{600nm} + 0.2609$ ($R^2 = 0.989$) Eq. (1).

2.3 Biosorption: kinetics and equilibrium study

Kinetic studies were accomplished in Erlenmeyer flasks containing 150 mL of the dye solution at a concentration of 50 mg L^{-1} and 0.5 g L^{-1} of yeast biomass. The flasks were placed on orbital shakers at a constant speed (120 rpm for 3 h) at 25 ºC. Aliquots were collected at regular time, centrifuged (10 000xg for 10 min) to remove the biosorbent and the concentration of dye was measured using the spectrophotometer Prim Light SECOMAM at $\lambda = 515_{nm}$. The biosorption was reported as decolorization rate (D%) (Eq. 2), and the biosorption capacity (Qt) was calculated according to Eq. 3.

D% = (A(i) -A(t)) / A(i) X 100 Eq. (2)

Qt = ((C(i)-C(t)) V / W) Eq. (3)

Where, A(i) and A(t) are lthe absorbance of dye-amended medium at the start point (i) and at a regular time (t); C(i) and C(t) are the initial and the equilibrium dye concentrations (mg L^{-1}); V is the volume of the solution (mL); and W is the weight of the biomass (g L^{-1}).

To explain and predict the kinetics of the yeast-dye biosorption interaction, various mathematical kinetic and isotherm models can be employed [15]. In this study, Lagergren's pseudo and pseudo-second-order were applied to define the type of interactions (physisorption or chemisorption), while the intra-particle diffusion model was used to describe the internal diffusion of dye in the cell wall. The isotherms were next applied in order to define the biosorption efficiency and to understand the relationship between the dye concentrations at its equilibrium concentration in the biosorbent solution [16]. The linear equations of kinetic and isotherm models used in the present study are summarized in Table 1.

Table 1
Linear equations of the kinetic and isothermal models used in the biosorption of AR14 by yeast biomass

Isotherm Model		Linear Equation	Representation Plot
	Freundlich	Log qe = Log K_F+ 1/n Log C_e	Log $q_e vs$ Log C_e
	Langmuir	$C_e/q_e = C_e/q_m + 1/K_L q_m$	$C_e/ q_e vs C_e$
Kinetic Model	*Pseudo first order*	Log(q_e-q_t) = Log(q_e) - (k_1/2.303)t	Log (q_e - q_t) vs t
	Pseudo second order	$(t/qt) = (k_2/k_2 qe^2) + (t/q_e)$	(t/q_t) vs t
	Intra particle diffusion	$qt = K_{id} t^{0.5} + C$	q_t vs $t^{0.5}$

Where, q_e is the sorption capacity at equilibrium (mg g^{-1}); C_e (mg L^{-1}) is the equilibrium concentration of the biosorbent; q_m is the maximum sorption capacity (mg g^{-1}); K_L is the Langmuir constant (L mg^{-1}); K_F is the Freundlich constant of the adsorption capacity and exponent n is the adsorption intensity which varies with the heterogeneity of the material.

2.4 Characterization of yeast biomass

2.4.1 Scanning electron microscopy with energy dispersive X-Ray analysis

SEM (JSM-IT500 InTouchScope™) was used to visualize the surface morphology of control and AR14-leaded cells, while the EDX was employed to analyze the elemental composition from the imaged area. The analytical conditions were as follows: Signal SED, magnification of x1 000-x55 000 landing voltage of 3.0 kV, work distance of 10.1 mm, at high vacuum mode.

2.4.2 Fourier-transform infrared spectroscopy analysis

In order to determine the functional groups on *W. anomalus* surface and their role in AR14 biosorption. Control and Ar14-loaded cells. were analyzed using an ABB Bomem FTLA 2000 spectrometer analyzer. The salt pellets were prepared using 1 mg of biomass and 149 mg of KBr. Samples were dried at 85 ºC for 24 h and compressed at 40 kN for 5 min to form pellets. Thirty-two scans were performed at a range of 400 to 4000 cm^{-1}, with 4 cm^{-1} of resolution for each sample.

2.4.3 Zeta potential and Zero-point charge measurement

The measurement of the zeta potential was achieved in order to determine the zeta potentials of the yeast cell as a function of pH from 3 to 10. Indeed, a volume of 100 mL of yeast suspension (0.05 g L^{-1}) was harvested by centrifugation at 10 000xg for 10 min, then the biomass was resuspended in 10 mL of 0.1 M NaCl. The initial pH of the suspensions was adjusted from 3 to 10 with 0.1 M of HCl or NaOH solutions. Next, the zeta potential was evaluated in the electrophoresis cell at 25 ºC with Nanosizer Nano (Malvern). For each pH value, triplicate measurements were taken, and for each data approximately, 30 readings were done [17]. The electrical state of yeast surface in solution was characterized using point of zero charge (pHzc). In fact, NaCl solutions (0.1 M) with pH ranging from 3 to 10 was prepared, then aliquots of 10 mL of each pH-adjusted NaCl solution were mixed with 0.05 g peat, shaken for 24 h at 25 ºC, and the final pH values were measured. The difference in ΔpH was plotted against the initial pHi to determine the pHzc [18].

2.4.4 Contact angle measurement

The measurement of the contact angle was carried out at 25 ºC as described by Asri et al. [19], using a digital optical contact angle (Data Physics OCA 40), via the sessile drop method, by using water, formamide and diiodomethane (Table S1). Both the left and the right contact angles measurements of algal biomasses were automatically calculated from the digitalized image using SCA 20 software. The degree of hydrophobicity of control and dye-leaded to cells of *W. anomalus* were then estimated according to Vogler's and Van Oss approach [20, 21].

2.5 Statistical analysis

All experiments were carried out in triplicate, and the results were recorded as the mean ± standard deviation. The statistical analysis of obtained data was performed using GraphPad Prism software version 8.0, with unpaired T-test. P-value of < 0.05 were perceived as statistically significant.

2.6 Optimization of biosorption using the design of experiments

2.6.1 Screening of factors using Plackett–Burman design (PBD)

Factors screening was performed using PBD [22] via MINITAB 18.1 software. The choice of the most influencing factors on the biosorption process was based on the literature research focusing on biosorption optimization with a one-factor-at-a-time approach. In fact, six variables were selected including temperature (ºC), pH, yeast dosage (g L^{-1}), dye concentration (mg L^{-1}), shaking speed (rpm) and contact time (min) at two levels (maximum (+ 1) and minimum (-1)) (Table S2). According to the adopted method, it was presumed that there is no parameters interaction. Hence, the data was modeled using the first-order multiple regression (Eq. 7).

$$Y = \beta_0 + \sum \beta_i X_{i\ (i = 1, \ldots, k)} \quad \text{Eq. (7)}$$

Where, (Y) is the biosorption response, (β_0) is the model intercept and (β_i) is the variable estimates. Thus, ANOVA and lack of fit were used for statistical significance. While the Fisher variation ratio (F) and the probability value (p) were used to select the effective parameters.

2.6.2 Optimization of biosorption parameters using Box-Behnken design (PBD)

Based on the PBD results, three variables have a significant effect on the biosorption process. Next, the Box-Behnken model was used for the biosorption optimization [23]. And the Eq. (8) was used to calculate the coded values of variables.

$$Xi = (x_i - x_0 / \Delta x),\ i = 1, 2, 3, \ldots k \quad \text{Eq. (8)}$$

Where, (Xi) is the dimensionless value of a process variable; (x_i) is the real value of an independent variable; (x_0) is the value of (x_i) at the center point; and (Δx) is the step change. The second order equation (Eq. (9)) was used in order to correlate the dependent and independent variables:

$$Y = b_0 + b_1A + b_2B + b_3C + b_{12}AB + b_{13}AC + b_{23}BC + b_{11}A^2 + b_{22}B^2 + b_{33}C^2 \quad \text{Eq. (9)}$$

Where, (Y) is the biosorption efficiency response; (b_0) is constant, (b_1, b_2 and b_3) are linear coefficients; (b_{12}, b_{13} and b_{23}) are cross product coefficients, and (b_{11}, b_{22}, and b_{33}) are quadratic coefficients; (A, B and C) are coded experimental levels of the selected variables of the screening phase. It was represented in terms of a three class levels (low (-1), central point (0) and high (+ 1)) (Table S3). The optimum values of each factor were calculated by solving the regression equation, evaluating the contour map, and setting up constraints on the variable levels [24]. The significance of the model is derived from the test of goodness-of-fit, mostly expressed as the coefficient of determination (R^2). p-value below to 0.05 was considered statistically significant [25].

3. Results And Discussion

3.1 Biosorption: kinetics and equilibrium study

Biosorption of AR14 onto *W. anomalus* biomass as a function of contact time, at four initial dye concentrations (50, 100, 150, and 200 mg L^{-1}) are depicted in Fig. 1. The result indicates that for all tested concentrations, the rate of biosorption increased with increasing contact time up to 10 min, after that, an equilibrium was reached. Indeed, three phases were recorded in the biosorption process of AR14 into the cell wall. At the beginning, a rapid biosorption rate occurred, thereafter the dye molecules biosorbed gradually until the maximum biosorption capacity of biosorbents was reached. The initial phase (5 min) can be attributed to the availability of large surface area and many vacant macropores for the dye uptake. Also, the dye biosorption at this phase was rapid, suggesting the involvement of a passive process like physical adsorption or ion exchange interaction on the cell surface. The second stage (5 to 10 min), was characterized by gradual and slow uptake. This result can be explained by the saturation of active functions groups on the cell surface [26]. As well as, by the repulsive forces among adsorbed dye molecules and those present in the solution [27]. At the third stage, the biosorption process reached equilibrium state. Similar findings were reported previously on the biosorption of Strazone blue [28], Acid blue 161 [29], and Direct red 23 [30] using *S. cerevisiae* biomass.

As shown in the Fig. 2B, the pseudo-first-order model was not applicable to the AR14-yeast biosorption system, there was no linearization of experimental data, and the R^2 of all the studied concentrations were less than 90% (Table 2) [31]. On the other hand, the R^2 value of the pseudo-second-order model was relatively close to 1 for all tested concentrations, suggesting therefore that this model seems to be a good fit for this biosorption system. Moreover, the values of Qe (cal) calculated were closer to the experimental values Qe (exp), confirming the goodness-of-fit of the model. The distinguished features of this model are: (i) the rate of biosorption is determined by adsorption capability rather than adsorbate concentration, (ii) it is well for the complete data range of contact time, and (iii) is in agreement with chemisorption being the rate-limiting step [32]. However, the pseudo-second order model did not identify the potential mechanism of diffusion into the pores. The kinetics were then analyzed through the intraparticle diffusion model. Indeed, the Q_t was plotted relative to the ($\sqrt{t}$) and are given in Fig. 2B, and the resulting kinetics parameters are given in Table 2. It has been shown that if biosorption follows an intraparticle diffusion model, the plot of (Qt) versus ($\sqrt{t}$) should be linear, and if the plot passes through the origin (C = 0), the adsorption kinetics follows the intraparticle diffusion model. However, if (C # 0), this indicates some degree of boundary layer control. The intraparticle diffusion model is not the rate control step of the biosorption process, but it can work simultaneously with other diffusion models [33]. As shown in the Fig. 2B, there are two linear regions representing the diffusion boundary layer, followed by intraparticle diffusion in macro pore [34]. This result demonstrates the occurrence of intraparticle diffusion and indicates that the yeast biomass reaches biosorption equilibrium when diffusion occurs in the macro pore layer, and the resistance to mass transfer is not involved in the dye uptake kinetics [35]. Kismir et Aroguz [36] reported that the process of mass transfer of dye onto the biosorbents can take place in

general through four steps: (i) bulk diffusion (transfer from bulk solution to the surface of the biosorbent), (ii) film diffusion (transfer through the boundary layer to the biosorbent surface), (iii) intra-particle diffusion (transfer from the surface to the interior pores of the particle), (iv) chemical reaction via ion-exchange, complexation, chelation; the adsorption of dye at an active site on the biosorbent surface.

Table 2
Kinetic parameters of AR14 biosorption on yeast biomass

Models	kinetics parameters	Initial dye concentrations (mg L^{-1})			
		50	100	150	200
Pseudo first order	K_1 (min^{-1})	0.205	0.194	0.215	0.195
	R^2	0.857	0.477	0.609	0.524
Pseudo second order	K_2 (g mg^{-1} min^{-1})	0.126	0.051	0.022	0.014
	R^2	0.999	0.999	0.999	0.998
	Qe (cal)	23.980	46.510	69.930	95.230
	Qe (exp)	24.038	50.000	67.129	92.082
Intra-particle diffusion	K_{i1}	7.847	14.66	21.65	29.190
	C_1	0.549	1.277	0.955	0.179
	R_1^2	0.983	0.974	0.993	0.999
	K_{i2}	0.030	0.083	0.022	0.028
	C_2	23.59	45.657	68.835	93.527
	R_2^2	0.920	0.254	0.148	0.035

According to the graphical representation of Langmuir and Freundlich isotherms (Fig. 3), and the corresponding models' constants listed in the Table 3, the R^2 was respectively at 0.954 and 0.849. We may conclude that Langmuir isotherms describe an appropriate fit to the biosorption of AR14 onto *W. anomalus* compared to Freundlich isotherms. Langmuir isotherms predict that the biosorption is based on monolayer adsorption on a homogeneous site without any interaction between biosorbed dye molecules on neighboring sites, it also assumes that there is equal energy for all sites, and that there are multiple biosorption sites for a specific surface, and when these sites are fully saturated, no further biosorption can take place [26, 37]. Aksu et Dönmez [31] reported the applicability of both Langmuir and

Freundlich models to the biosorption system of Remazol Blue reactive dye into dried cells of *Candida* strains.

Table 3
Biosorption isotherm models and their corresponding parameters for the biosorption AR14 by *W. anomalus* biomass

Langmuir			***Freundlich***		
Q_{max} (mg g^{-1})	K_L (L mg^{-1})	R^2	1/n	K_f	R^2
126.58	0.107	0.954	0.5	15.87	0.849

3.2 Characterization of yeast biomass

3.2.1 SEM coupled with EDX analysis

SEM and EDX analysis were used to establish the changes in morphology and the elemental composition of the yeast biomass before AR14 biosorption, with a view to establish the mechanism of dye binding to the cell wall. The Fig. 4A shows the SEM images of colorless yeast cells, and the Fig. 4B shows *W. anomalus* after AR14 biosorption in 8000× magnification. There were notable differences in cellular morphology between the control and AR14-loaded cells. The yeast cells prior to AR14 biosorption had a normal shape and a transparent outer layer outside the cell surface. However, after biosorption of the dye molecules, the cell becomes smooth and presents hazy textures. Furthermore, the X-ray spectra showed a difference in the intensity of elementary peaks of C, O, P, and K after dye biosorption.

3.2.2 FTIR spectroscopy analysis

The FTIR spectra (Fig. 5) of *W. anomalus* biomass before and after AR14 biosorption were used to identify the involved functional groups of the cell wall in the dye-biosorption process [38]. The strong vibration around 3000–3500 cm^{-1} indicates the existence of stretching vibration of hydroxyl (-OH) and/or amino (-NH_2) groups, which are among the functional groups of chitosan and amino acids on the cell wall of *W. anomalus* [39]. The peaks at 2854–2923 cm^{-1} are in the region of the absorption of lipid acyl chains (3050 – 2800 cm^{-1}) that correspond to symmetric and asymmetric stretching of methylene and methyl groups in the membrane phospholipids [40]. The strong peaks at 1642 cm^{-1} detected in the region between 1700 and 1500 cm^{-1} indicate the presence of amide (I and II) bands, mainly from protein peptide bonds (C = O stretching and N-H bending), corresponding to several uronic acids and amino acids present in the cell wall [41]. The infrared absorption in the spectral at 1406 cm^{-1} may be caused by the sulfur (-SO-) and phosphorous (-PO-) groups, which range between 1500 and 1300 cm^{-1} corresponding to vibrations of fatty acids and proteins [39]. The bands observed at 1073 cm^{-1} are assigned to C–O stretching vibration of alcohols and carboxylic acids which are mainly related to complex vibrations from

carbohydrates [42]. Furthermore, after AR14-biosorption, a significant change was noticed in the transmittance of these functional groups which may be attributed to its occupation by dye molecule. Based on the comparison of the spectra before and after AR14 biosorption, there were also a shift in various bands, which represented the groups involved in the biosorption corresponding to hydroxyl, carboxylic acid, amine and amino groups. Some previous studies indicated also that the biosorption process is accomplished by chelation and formation of ionic bridges between dye molecules and functional groups. The binding mechanism of dye molecules to the yeast cell is explained by the strong attractive forces of peptidomannan, peptidoglycan, lipids and heteropolysaccharides..., which contains several functional groups such as carboxyl, hydroxyl, amino, phosphate, and other charged groups [43, 44]. In line with our findings, it has been reported by Dilarri et al. [29] that the biosorption of synthetic dyes by the cell wall of *S. cerevisiae* involved some amide and amine groups, and demonstrated that the vibration of (–C = O) and (–C–O) can be another linking group in the chitin structure. Moreover, it can be predicted according to the FTIR analysis that Yoshida H-binding, dipole–dipole H-binding, π–π and n–π interactions play an indispensable role in the AR14 biosorption onto yeast cell [45]. The cell wall architecture and the proposed mechanisms of AR14 biosorption are illustrated in Fig. 6. In fact, the major components of the *S. cerevisiae* cell wall are β-glucans (formed by 1,3-β- and 1,6-linkages) and mannoproteins (proteins highly N- or O-glycosylated mannose residues linked by 1,2,-1,3-, 1,4- and 1,6-α-linkages), which represent about 50–60% and 40–50%, respectively of the cell wall mass, as well as 1–3% for the chitin, which is manufactured by 1,4-β-N-acetylglucosamine [46]. These complex macromolecular structures present potential binding sites for diverse pollutants including toxic dye molecules [47].

3.2.3 Zeta potential and Zero-point charge measurement

The electrical state of the cell surface is one of the critical parameters in biosorption studies. Thus, the measurement of zeta potential can be one of the key parameters related to the external loads of the adsorbent [48]. As shown in Fig. 7A, the zeta potential of *W. anomalus* biomass was maintained at a negative charge, regardless of the initial pH value, and it varied from − 4.6 mV at pH 3 to -9.28 at pH 10. This can testify the anionic characteristics and the high concentration of acid functional groups on the surface of *W. anomalus*. These results are consistent with previous studies that evaluated the zeta potential of different yeast strains [49, 50]. It is known that there was a close relationship between the zeta potential of biomaterials and their biosorption capacity [51]. On the other hand, the value of pHzc at which ΔpH = 0 was found at 5.25 (Fig. 7B) confirmed thus the presence of anionic groups on the cell surface that dominate over the cationic groups. Zehra et al. [18] reported that the acidic value of pHzc of baker's yeast, was attributed to the presence of various biopolymers on the yeast cell wall, mainly β-glucan and chitosan, that may have caused a substantial load on the external surface of the cells and given a net charge on the surface that depending on the pH caused by deprotonation of functional groups in the cell wall [52, 53]. The number of positively charged sites decreases, when the pH of the solution increases. The decrease in the biosorption of AR14 anions is a result of the electrostatic repulsion forces of the negatively charged cell surface at acidic pH condition [54].

3.2.4 Contact angle measurements

Based on both Vogler's and Van Oss approaches, *W. anomalus* exhibited a hydrophilic character, the θ_w value (34.9 ° ± 0.4) was less than 65 °, and the ΔGiwi had a positive value (37.23 ± 1.13 mJ m^{-2}). These findings agree with previous results reporting the hydrophilic character of various yeast strain [55, 56]. In fact, yeast surface hydrophobicity has been shown to be related to the proteins of cell surface [57, 58]. In addition, *W. anomalus* appear to behave predominantly as electron donors/Lewis bases with high values of γ^- = 52.57 ± 0.6 mJ m^{-2} (Table 4). These results also indicate that this strain exhibit weak electron acceptor characters with γ^+ = 0.24 ± 0.07 mJ m^{-2}. Some previous research showed also that microbial cell surfaces are mainly electron donating, while electron-accepting cell surfaces are rarely found [59], which may be due to the presence of phosphate groups in cell wall [57]. Theses finding are consistent with the FTIR analyses of *W. anomalus*, that confirm the presence of phosphate groups on its cell surface. On the other hand, the θ_w of *W. anomalus* significantly decreased from 34.9 º ± 0.4 to 31.6 º ± 0.9 after dye biosorption (Table 4). This may be attributed to an increase in the density of polar functional groups on the biomass surfaces after the biosorption process [60]. In addition, a significant variation was noted in the electron donor and acceptor character after dye biosorption (γ^+ from 0.24 ± 0.07 to 0.08 ± 0.02 mJ m^{-2}; and γ^- from 52 57 ± 0.6 to 59.79 ± 0.5 mJ m^{-2}) which can be attributed to the interaction of cell surface functional groups with dye molecules.

Table 4
Contact angle values using water (θ_w), formamide (θ_F) and diiodomethane (θ_D), Lifshitz-vander Waals (γ^{LW}), electron-donor (γ^-) and electron-acceptor (γ^+) parameters, surface energies (ΔGiwi) of *W. anomalus* cells before and after AR14 biosorption

	Contact angles (°)			Surface tension: components and parameters (mJ m^{-2})			Surface energies
	θ_w	θ_F	θ_D	γ^{LW}	γ^+	γ^-	ΔGiwi (mJ m^{-2})
Raw Biomass	34.9 ± 0.4	42.2 ± 0.6	49.5 ± 1.6	34.45 ± 0.9	0.24 ± 0.07	52.57 ± 0.6	37.23 ± 1.13
AR14-Biomass	31.6 ± 0.9*	44.1 ± 0.5ns	36.3 ± 0.6***	41.33 ± 0.3***	0.08 ± 0.02*	59.79 ± 0.5***	44.9 ± 1.2**
*statistical significance p value < 0.05							

3.3 Optimization of the biosorption by using the design of experiments

3.3.1 Factor's screening using Plackett–Burman design

Based on the positive or negative values of the factors modeled on Eq. 10, the factors A and C have positive values, indicating, therefore, their synergistic effect to the biosorption response, while the other negative factors indicate an antagonistic effect.

$$D\ \% = 11.0 + 0.933\ A - 3.64\ B + 12.89\ C - 0.003\ D - 0.207\ E + 0.774\ F \quad \text{Eq. (10)}.$$

Table 5 represents the value of the regression coefficients, t-tests, and p-values for the six independent variables. The multiple correlation coefficient R^2 of the first-order model indicates that 75.82% of the data variance could be estimated by the model. Yet, the difference between the predicted R^2 (51.80%) and adjusted R^2 (67.28%) indicated that it is impossible to evaluate the relationship between the significant independent variables and the response based on the first-order model. As illustrated in Fig. 8A, the biomass dosage (89.06%), pH (26.57%), and the dye concentration (10.94%) are significant influence factors on biosorption capacity. Indeed, the increase in the yeast dosage showed a positive influence, while increasing dye concentration and pH had a negative influence on the efficiency of AR14 biosorption (Fig. 8B). Several studies reported that an increase in biomass dosage significantly improves the biosorption capacity, due to the increase of exchangeable sites present in the cell wall [24]. Evidently, pH is also one of the factors controlling the biosorption process. In fact it can affect the chemistry of dye molecules, the physicochemical properties of the yeast surface and the magnitude of electrostatic charges imparted by the ionized dye molecules [61]. It has been documented that the optimal biosorption pH of particular dyes depends closely on their chemical properties. For instance, the biosorption of reactive dyes requires an acidic conditions, whereas basic dyes requires neutral or alkaline conditions [28]. In addition, the net charge of the biosorbent is also pH dependent, at a low pH value, the functional group on the cell surface becomes protonated and acquires a net positive charge increasing thereby the binding of anionic dyes. Regarding the effect of the initial dye concentration on the biosorption capacity, its closely depending on the binding sites available on the biomass surface. Moreover, it has been reported that a high dye solute uptake can be obtained at a high initial dye concentration, which is linked to the high driving force for mass transfer [62, 63]. However, at lower initial dye concentrations, the biosorption becomes independent of the initial dye concentration, because the ratio of the initial moles of the solute to the available area becomes low [64].

Table 5
ANOVA for process variables of the PBD

Source	DF	Adj SS	Adj MS	F-Value	P-Value
Model	6	10216.7	1702.79	8.88^{***}	0.000
Linear	6	10216.7	1702.79	8.88^{***}	0.000
Temperature (ºC) (A)	1	751.4	751.39	3.92^{NS}	0.064
pH (B)	1	1272.1	1272.06	6.64^{**}	0.02
Biomass dosage ($g.L^{-1}$)) (C)	1	2241.6	2241.58	11.69^{**}	0.003
Agitation (rpm) (D)	1	0.8	0.82	0.00^{NS}	0.949
Dye (mg L^{-1}) (E)	1	5821.6	5821.58	30.37^{***}	0.000
Contact time (min) (F)	1	129.3	129.30	0.67^{NS}	0.423
Error	17	3258.8	191.69		
Lack-of-Fit	5	1860.8	372.16	3.19^{*}	0.046
Pure Error	12	1398.0	116.50		
Total	23	13475.5			
R^2 75.82; Adjusted R^2 67.28; Predicted R^2 51.80%.					
DF: degrees of freedom; SS: sum of squares; MS: mean sum of squares,					
*Significance (α = 0.05)					

3.3.2 Optimization of process parameters using Box-Behnken model

The Eq. (11) model the relationship between the predicted biosorption response and the process parameters with the second-order polynomial equation. In fact, the negative values of both factors (A) and (C) indicates that a high biosorption efficiency occurs at lower dye concentration and at acidic pH solution.

D% = 70.8–0.243 A + 48.99 B – 23.18 C – 0.00015 A*A -10.50 B*B + 1.625 C*C + 0.0001 A*B + 0.0419 A*C – 2.61 B*C Eq. (11)

As illustrated in the Table 6, the regression of the quadratic model was statistically significant (F = 21.48; P = 0.00), at 95% confidence limits. The R^2 indicates that the model as fitted explains 90.62% of the variability, suggesting a significant correlation between the predicted and experimental effects of the selected variables. Furthermore, the predicted R^2 value (76.27%) was in line with the founded R^2value (86.41%) of the adjusted, indicating that 10.14% of the variability in the response was not explainable by this model. Also, the F value was significantly proportional to the pure error, and the F values for the factors A, B and C were at 17.44, 42.69, and 79.62, respectively, showing consequently that the pH of the solution was most significantly different from zero at the 95.0% confidence level followed by the biomass dosage and dye concentration (Fig. 9A). Consistent with the results of the factor selection step, the normalized effects indicate that increasing the yeast dose had a positive influence, whereas a negative influence on biosorption efficiency was observed when increasing the dye concentration or initial pH of the medium (Fig. 9B). The contour plots displaying the variation of AR14-biosorption, with respect to the simultaneous shift in two factors, indicates the relationship and the interaction impact of two variables with varying concentrations on the biosorption, while the third variable is apprehended at the central point. As described in the Fig. 10A, when the initial pH was maintained at 5, the biosorption rate was proportional to the increase in the biomass dosage, but inversely proportional to the increase in the initial dye concentration. Meanwhile, when the initial dye concentration was maintained at 125 mg L^{-1} (Fig. 10B), the rate of biosorption was proportional to the increase in the biomass dosage, and the optimum biosorption was achieved at a lower pH level. Similarly, when the biomass dosage was maintained at 1.125 mg L^{-1} (Fig. 10C), the optimum biosorption level was proportional to the initial pH of the medium and the initial dye concentration. Higher biosorption was achieved at acidic conditions with lower dye concentration. El-Naggar et al. [65] reported that the dye biosorption system was depends on protonation or deprotonation of various functional groups on the cell surface. At pH 3–4, the protonation of amino groups on the yeast cell wall increases the net positive charge and enhances the biosorption of negatively charged dye ions by electrostatic binding.

Table 6
Analysis of variance for response surface quadratic model.

Source	DF	Adj SS	Adj MS	F-Value	P-Value
Model	9	3821.96	424.66	21.48^{***}	0.000
Linear	3	2762.70	920.90	46.58^{***}	0.000
Dye (mg L^{-1})(A)	1	344.76	344.76	17.44^{***}	0.000
Biomass (g L^{-1}) (B)	1	843.87	843.87	42.69^{***}	0.000
pH (C)	1	1574.06	1574.06	79.62^{***}	0.000
Square	3	620.61	206.87	10.46^{***}	0.000
A * A	1	3.03	3.03	0.15^{NS}	0.700
B * B	1	257.68	257.68	13.03^{**}	0.002
C * C	1	312.17	312.17	15.79^{***}	0.001
2-Way Interaction	3	438.65	146.22	7.40^{**}	0.002
A * B	1	0.00	0.00	0.00^{NS}	0.997
A * C	1	315.76	315.76	15.97^{***}	0.001
B * C	1	122.89	122.89	6.22^{**}	0.022
Error	20	395.38	19.77		
Lack-of-Fit	3	361.66	120.55	60.77^{***}	0.000
Pure Error	17	33.72	1.98		
Total	29	4217.34			
R^2 90,62; Adjusted R^2 86,41; Predicted R^2 76,27%.					

4. Conclusion

The present study shows that *W. anomalus* can be used as an effective biosorbent for the removal of AR14 dye from an aqueous solution. At the beginning of the biosorption process, the bioremoval occurred rapidly, then proceeded gradually to reach the equilibrium state. The studied isotherm model indicated a monolayer adsorption of AR14 molecules at homogeneous sites on the cell wall surface of *W. anomalus*. Furthermore, biosorption kinetic modelling followed both pseudo-second order as well as the intraparticle diffusion model. The characterization of yeast biomass before and after dye biosorption indicated that

the bioremoval was attributed to the presence of various active groups on the cell surface, the zeta potential of *W. anomalus* was at a negative charge, and the acidic value of pHzc confirmed the presence of anionic groups on the cell surface that dominate over the cationic groups. The adsorbate concentration and the adsorbent dosage ratio as well as the initial pH has significantly affected the biosorption efficiency. The optimum condition for maximum dye biosorption was achieved at pH 3–4, with lower initial dye concentrations (50–75 mg L^{-1}) and yeast biomass greater than 1.25 g L^{-1}. Until today, very few studies have been conducted on the use of yeasts as biosorbent. The majority of this research is limited to the laboratory scale. Thus, the emergence of this new research theme that could be part of future solutions suggested for the treatment of colored effluents.

Declarations

Availability of data and materials

The data used to support the findings of this study are available from the corresponding author upon request.

Competing interests

The authors declare they have no competing interests.

Funding

Not Applicable

Authors' contributions

M. Danouche: Conceptualization, Methodology, Formal analysis, Writing - original draft, Visualization. H. El Arroussi: Supervision, review & editing, Validation, Resources, Funding acquisition. N. El Ghachtouli: Supervision, review & editing, Project administration.

Acknowledgements

The authors gratefully acknowledge the Moroccan Foundation for Advanced Science, Innovation and Research (MAScIR), and Regional University Centre of Interface (CURI), Sidi Mohamed Ben Abdellah University for their financial and technical support.

References

1. T.R. Waghmode, M.B. Kurade, A.N. Kabra, S.P. Govindwar, Degradation of remazol red dye by *Galactomyces geotrichum* MTCC 1360 leading to increased iron uptake in *Sorghum vulgare* and *Phaseolus mungo* from soil, Biotechnol. Bioprocess Eng. 17 (2012) 117–126. https://doi.org/10.1007/s12257-011-0307-0.

2. R.G. Saratale, G.D. Saratale, J.S. Chang, S.P. Govindwar, Bacterial decolorization and degradation of azo dyes: A review, J. Taiwan Inst. Chem. Eng. 42 (2011) 138–157. https://doi.org/10.1016/j.jtice.2010.06.006.
3. Y. Fu, T. Viraraghavan, Fungal decolorization of dye wastewaters: a review, Bioresour. Technol. 79 (2001) 251–262. https://doi.org/10.1556/034.58.2016.1-2.6.
4. S. Arslan, M. Eyvaz, E. Gürbulak, E. Yüksel, A Review of State-of-the-Art Technologies in Dye-Containing Wastewater Treatment – The Textile Industry Case, in: Text. Wastewater Treat., InTech, 2016: pp. 3–28. https://doi.org/http://dx.doi.org/10.5772/64140.
5. M.T. Yagub, T.K. Sen, S. Afroze, H.M. Ang, Dye and its removal from aqueous solution by adsorption: a review., Adv. Colloid Interface Sci. 209 (2014) 172–84. https://doi.org/10.1016/j.cis.2014.04.002.
6. G. Crini, E. Lichtfouse, L.D. Wilson, N. Morin-Crini, Conventional and non-conventional adsorbents for wastewater treatment, Environ. Chem. Lett. 17 (2019) 195–213. https://doi.org/10.1007/s10311-018-0786-8.
7. A. Srinivasan, T. Viraraghavan, Decolorization of dye wastewaters by biosorbents: A review, J. Environ. Manage. 91 (2010) 1915–1929. https://doi.org/10.1016/j.jenvman.2010.05.003.
8. Z. Aksu, S. Tezer, Biosorption of reactive dyes on the green alga *Chlorella vulgaris*, Process Biochem. 40 (2005) 1347–1361. https://doi.org/10.1016/j.procbio.2004.06.007.
9. N. Jafari, M.R. Soudi, R. Kasra-Kermanshahi, Biodecolorization of textile azo dyes by isolated yeast from activated sludge: Issatchenkia orientalis JKS6, Ann. Microbiol. 64 (2014) 475–482. https://doi.org/10.1007/s13213-013-0677-y.
10. R. de C.M. d. Miranda, E. de B. Gomes, N. Pereira, M.A. Marin-Morales, K.M.G. Machado, N.B. de Gusmão, Biotreatment of textile effluent in static bioreactor by *Curvularia lunata* URM 6179 and Phanerochaete chrysosporium URM 6181, Bioresour. Technol. 142 (2013) 361–367. https://doi.org/10.1016/j.biortech.2013.05.066.
11. K. Singh, S. Arora, Removal of synthetic textile dyes from wastewaters: A critical review on present treatment technologies, Crit. Rev. Environ. Sci. Technol. 41 (2011) 807–878. https://doi.org/10.1080/10643380903218376.
12. S.K. Sen, S. Raut, P. Bandyopadhyay, S. Raut, Fungal decolouration and degradation of azo dyes: A review, Fungal Biol. Rev. 30 (2016) 112–133. https://doi.org/10.1016/j.fbr.2016.06.003.
13. E. V. Soares, H.M.V.M. Soares, Bioremediation of industrial effluents containing heavy metals using brewing cells of *Saccharomyces cerevisiae* as a green technology: A review, Environ. Sci. Pollut. Res. 19 (2012) 1066–1083. https://doi.org/10.1007/s11356-011-0671-5.
14. W. Bahafid, N.T. Joutey, H. Sayel, M. Iraqui-Houssaini, N. El Ghachtouli, Chromium adsorption by three yeast strains isolated from sediments in morocco, Geomicrobiol. J. 30 (2013) 422–429. https://doi.org/10.1080/01490451.2012.705228.
15. M. Danouche, H. El Arroussi, W. Bahafid, N. El Ghachtouli, H. El Arroussi, W. Bahafid, N.E.G. An, An overview of the biosorption mechanism for the bioremediation of synthetic dyes using yeast cells, Environ. Technol. Rev. 10 (2021) 58–76. https://doi.org/10.1080/21622515.2020.1869839.

16. I. Morosanu, C. Teodosiu, C. Paduraru, D. Ibanescu, L. Tofan, Biosorption of lead ions from aqueous ef fl uents by rapeseed biomass, N. Biotechnol. (2016). https://doi.org/10.1016/j.nbt.2016.08.002.
17. S. Hadjoudja, V. Deluchat, M. Baudu, Journal of Colloid and Interface Science Cell surface characterisation of *Microcystis aeruginosa* and *Chlorella vulgaris*, J. Colloid Interface Sci. 342 (2010) 293–299. https://doi.org/10.1016/j.jcis.2009.10.078.
18. T. Zehra, N. Priyantha, L.B.L. Lim, Removal of crystal violet dye from aqueous solution using yeast-treated peat as adsorbent: thermodynamics, kinetics, and equilibrium studies, Environ. Earth Sci. 75 (2016) 1–15. https://doi.org/10.1007/s12665-016-5255-8.
19. M. Asri, N. El, S. Elabed, S. Ibnsouda, A. Elabed, B. Silva, T. Tavares, W*icherhamomyces anomalus* biofilm supported on wood husk for chromium wastewater treatment, J. Hazard. Mater. 359 (2018) 554–562. https://doi.org/10.1016/j.jhazmat.2018.05.050.
20. E.A. Vogler, Structure and reactivity of water at biomaterial surfaces, Adv. Colloid Interface Sci. 74 (1998) 69–117. https://doi.org/10.1016/S0001-8686(97)00040-7
21. C.J. Van Oss, M.K. Chaudhury, R.J. Good, Interfacial Lifshitz-van der Waals and polar interactions in macroscopic systems, Chem. Rev. 88 (1988) 927–941. https://doi.org/10.1021/cr00088a006.
22. Plackett, R. L., & Burman, J. P. The design of optimum multifactorial experiments. *Biometrika*, *33*(4), (1946) 305–325. https://doi.org/doi:10.2307/2332195.
23. G.E.P. Box, D.W. Behnken, Some new three level design for study of quantitative variables, Technometrics. 2 (1960) 455–475. https://doi.org/10.2307/1266454
24. M. Kousha, E. Daneshvar, H. Dopeikar, D. Taghavi, A. Bhatnagar, Box-Behnken design optimization of Acid Black 1 dye biosorption by different brown macroalgae, Chem. Eng. J. 179 (2012) 158–168. https://doi.org/10.1016/j.cej.2011.10.073.
25. K. Papadopoulou, I.M. Kalagona, A. Philippoussis, F. Rigas, Optimization of fungal decolorization of azo and anthraquinone dyes via Box-Behnken design, Int. Biodeterior. Biodegrad. 77 (2013) 31–38. https://doi.org/10.1016/j.ibiod.2012.10.008.
26. E. Daneshvar, A. Vazirzadeh, A. Bhatnagar, Biosorption of methylene blue dye onto three different marine macroalgae: Effects of different parameters on isotherm, kinetic and thermodynamic, Iran. J. Sci. Technol. Trans. A Sci. 43 (2019) 2743–2754. https://doi.org/10.1007/s40995-019-00764-8.
27. C. Smaranda, D. Bulgariu, M. Gavrilescu, An investigation of the sorption of Acid Orange 7 from aqueous solution onto soil, Environ. Eng. Manag. J. 8 (2009) 1391–1402. https://doi.org/10.30638/eemj.2009.203.
28. J.Y. Farah, N.S. El-Gendy, L.A. Farahat, Biosorption of Astrazone Blue basic dye from an aqueous solution using dried biomass of Baker's yeast., J. Hazard. Mater. 148 (2007) 402–8. https://doi.org/10.1016/j.jhazmat.2007.02.053.
29. G. Dilarri, É.J.R. de Almeida, H.B. Pecora, C.R. Corso, Removal of dye toxicity from an aqueous solution using an industrial strain of *Saccharomyces cerevisiae* (Meyen), Water. Air. Soil Pollut. 227 (2016). https://doi.org/10.1007/s11270-016-2973-1.

30. L.G. Morão, G. Dilarri, C.R. Corso, Immobilization of *Saccharomyces cerevisiae* cells on *Luffa cylindrica*: a Study of a novel material for the adsorption of textile dye, Water. Air. Soil Pollut. 228 (2017) 228–248. https://doi.org/10.1007/s11270-017-3433-2.
31. Z. Aksu, G. Dönmez, A comparative study on the biosorption characteristics of some yeasts for Remazol Blue reactive dye, Chemosphere. 50 (2003) 1075–1083. https://doi.org/10.1016/S0045-6535(02)00623-9.
32. M. Davranche, C. Veclin, A.C. Pierson-Wickmann, H. El Hadri, B. Grassl, L. Rowenczyk, A. Dia, A. Ter Halle, F. Blancho, S. Reynaud, J. Gigault, Are nanoplastics able to bind significant amount of metals? The lead example, Environ. Pollut. 249 (2019) 940–948. https://doi.org/10.1016/j.envpol.2019.03.087.
33. F.C. Wu, R.L. Tseng, R.S. Juang, Initial behavior of intraparticle diffusion model used in the description of adsorption kinetics, Chem. Eng. J. 153 (2009) 1–8. https://doi.org/10.1016/j.cej.2009.04.042.
34. Y.S. Ho, G. McKay, Kinetic models for the sorption of dye from aqueous solution by wood, Process Saf. Environ. Prot. 76 (1998) 183–191. https://doi.org/10.1205/095758298529326.
35. H. Ka Yee, G. McKay, Y. King Lun, Selective adsorbents from chemically modified ordered mesoporous silica, Langmuir. 19 (2003) 3019–3024. https://doi.org/10.1016/s0167-2991(04)80581-0.
36. Y. Kismir, A.Z. Aroguz, Adsorption characteristics of the hazardous dye Brilliant Green on Saklıkent mud, Chem. Eng. J. 172 (2011) 199–206. https://doi.org/10.1016/j.cej.2011.05.090.
37. K.C. de Castro, A.S. Cossolin, H.C. Oliveira dos Reis, E.B. de Morais, Biosorption of anionic textile dyes from aqueous solution by yeast slurry from brewery, Brazilian Arch. Biol. Technol. 60 (2017) 1–13. https://doi.org/10.1590/1678-4324-2017160101.
38. P.M.G. Pugazhenthi, Adsorption of crystal violet dye from aqueous solution using mesoporous materials synthesized at room temperature, (2009) 390–405. https://doi.org/10.1007/s10450-009-9156-y.
39. A. Paula, G. Maria, A. Gabriela, F. Zielinski, M. Vieira, C. Windson, I. Haminiuk, Biosorption of anthocyanins from grape pomace extracts by waste yeast: kinetic and isotherm studies, J. Food Eng. 169 (2016) 53–60. https://doi.org/10.1016/j.jfoodeng.2015.08.016.
40. D. Ami, R. Posteri, P. Mereghetti, D. Porro, S.M. Doglia, P. Branduardi, Fourier transform infrared spectroscopy as a method to study lipid accumulation in oleaginous yeasts, Biotechnol. Biofuels. (2014) 7–12. https://doi.org/https://doi.org/10.1186/1754-6834-7-12.
41. Y. Zhang, W. Liu, M. Xu, F. Zheng, M. Zhao, Study of the mechanisms of Cu 2 + biosorption by ethanol / caustic-pretreated baker ' s yeast biomass, J. Hazard. Mater. 178 (2010) 1085–1093. https://doi.org/10.1016/j.jhazmat.2010.02.051.
42. G. Naja, B. Volesky, The Mechanism of Metal Cation and Anion Biosorption. In Microbial biosorption of metals (pp. 19–58)., Springer, Dordrecht, 2011. https://doi.org/10.1007/978-94-007-0443-5.

43. G.M. Gadd, Biosorption: Critical review of scientific rationale, environmental importance and significance for pollution treatment, J. Chem. Technol. Biotechnol. 84 (2009) 13–28. https://doi.org/10.1002/jctb.1999.
44. V. Vitor, C.R. Corso, Decolorization of textile dye by *Candida albican*s isolated from industrial effluents, J. Ind. Microbiol. Biotechnol. 35 (2008) 1353–1357. https://doi.org/10.1007/s10295-008-0435-5.
45. N.H. Tran, S. You, A. Hosseini-bandegharaei, Mistakes and inconsistencies regarding adsorption of contaminants from aqueous solutions: A critical review, Water Res. 120 (2017) 88–116. https://doi.org/10.1016/j.watres.2017.04.014.
46. G.G. Stewart, The Structure and Function of the Yeast Cell Wall, Plasma Membrane and Periplasm, in: Brew. Distill. Yeasts, Springer, Cham., 2017: pp. 55–75. https://doi.org/https://doi.org/10.1007/978-3-319-69126-8_5.
47. M. Fomina, G.M. Gadd, Biosorption: Current perspectives on concept, definition and application, Bioresour. Technol. 160 (2014) 3–14. https://doi.org/10.1016/j.biortech.2013.12.102.
48. T. Akar, B. Anilan, A. Gorgulu, S. Tunali, Assessment of cationic dye biosorption characteristics of untreated and non-conventional biomass: *Pyracantha coccinea* berries, 168 (2009) 1302–1309. https://doi.org/10.1016/j.jhazmat.2009.03.011.
49. S.M. Tazhibaeva, K.B. Musabekov, A.B. Orazymbetova, A.A. Zhubanova, Surface Properties of Yeast Cells, Colloid J. 65 (2003) 122–124. https://doi.org/https://doi.org/10.1023/A:1022391613491.
50. M.R. Lin, D. Q., Brixius, P. J., Hubbuch, J. J., Thömmes, J., & Kula, Biomass/adsorbent electrostatic interactions in expanded bed adsorption: a zeta potential study, Biotechnol. Bioeng. 83 (2003) 149–157. https://doi.org/10.1002/bit.10654.
51. M. Dundar, C. Nuhoglu, Y. Nuhoglu, Biosorption of Cu (II) ions onto the litter of natural trembling poplar forest, 151 (2008) 86–95. https://doi.org/10.1016/j.jhazmat.2007.05.055.
52. F.M. Klis, P. Mol, K. Hellingwerf, S. Brul, Dynamics of cell wall structure in *Saccharomyces cerevisiae*, FEMS Microbiol. Rev. 26 (2002). https://doi.org/10.1111/j.1574-6976.2002.tb00613.x
53. R. Garcia-rubio, H.C. De Oliveira, J. Rivera, G.A. Niño-vega, R.A. Hall, The Fungal Cell Wall: *Candida*, *Cryptococcus*, and *Aspergillus* Species, 10 (2020) 1–13. https://doi.org/10.3389/fmicb.2019.02993.
54. S. Tunali, A. Gorgulu, Z. Kaynak, B. Anilan, T. Akar, Biosorption of Reactive Blue 49 dye under batch and continuous mode using a mixed biosorbent of macro-fungus Agaricus bisporus and T*huja orientalis cones*, Chem. Eng. J. 148 (2009) 26–34. https://doi.org/10.1016/j.cej.2008.07.027.
55. M.S. Lucas, C. Amaral, A. Sampaio, J.A. Peres, A.A. Dias, Biodegradation of the diazo dye Reactive Black 5 by a wild isolate of *Candida oleophila*, Enzyme Microb. Technol. 39 (2006) 51–55. https://doi.org/10.1016/j.enzmictec.2005.09.004.
56. G. Vaca-medina, H. Martin-yken, A. Vernhet, P. Schmitz, M. Mercier-bonin, Shear-flow induced detachment of *Saccharomyces cerevisiae* from stainless steel: Influence of yeast and solid surface properties, Colloids Surfaces B Biointerfaces. 49 (2006) 126–135. https://doi.org/10.1016/j.colsurfb.2006.03.001.

57. S. Vichi, J.J. Gallardo-chacón, R. Pradelles, D. Chassagne, E. López-tamames, S. Buxaderas, Surface properties of *Saccharomyces cerevisiae* lees during sparkling wine ageing and their effect on flocculation, Int. J. Food Microbiol. 140 (2010) 125–130. https://doi.org/10.1016/j.ijfoodmicro.2010.04.009.
58. G. Suzzi, P. Romano, L. Vannini, Cell surface hydrophobicity and flocculence in *Saccharomyces cerevisiae* wine yeasts ', Colloids Surfaces B Biointerfaces. 2 (1994) 505–510.
59. H.C. Van Der Mei, R. Bos, H.J. Busscher, A reference guide to microbial cell surface hydrophobicity based on contact angles, Colloids Surfaces B Biointerfaces. 11 (1998) 213–221. https://doi.org/doi:10.1016/s0927-7765(98)00037-x.
60. Legorreta-Castañeda, A. J., Lucho-Constantino, C. A., Beltrán-Hernández, R. I., Coronel-Olivares, C., & Vázquez-Rodríguez, G. A. (2020). Biosorption of water pollutants by fungal pellets. Water, 12(4), 1155. https://doi.org/10.3390/w12041155
61. Y. Fu, T. Viraraghavan, Removal of Congo Red from an aqueous solution by fungus *Aspergillus niger*, Adv. Environ. Res. 7 (2002) 239–247. https://doi.org/10.1016/S1093-0191(01)00123-X.
62. A.R. Binupriya, M. Sathishkumar, D. Kavitha, K. Swaminathan, S.E. Yun, Aerated and rotated mode decolorization of a textile dye solution by native and modified mycelial biomass of *Trametes versicolor*, J. Chem. Technol. Biotechnol. 82 (2007) 350–359. https://doi.org/10.1002/jctb.
63. Y. Bulut, H. Aydin, A kinetics and thermodynamics study of methylene blue adsorption on wheat shells, Desalination. 194 (2006) 259–267. https://doi.org/10.1016/j.desal.2005.10.032.
64. K. Vijayaraghavan, Y.S. Yun, Bacterial biosorbents and biosorption, Biotechnol. Adv. 26 (2008) 266–291. https://doi.org/10.1016/j.biotechadv.2008.02.002.
65. N. El, A. El, Eco – friendly approach for biosorption of Pb 2 + and carcinogenic Congo red dye from binary solution onto sustainable *Ulva lactuca* biomass, Sci. Rep. (2020) 1–22. https://doi.org/10.1038/s41598-020-73031-1.

Figures

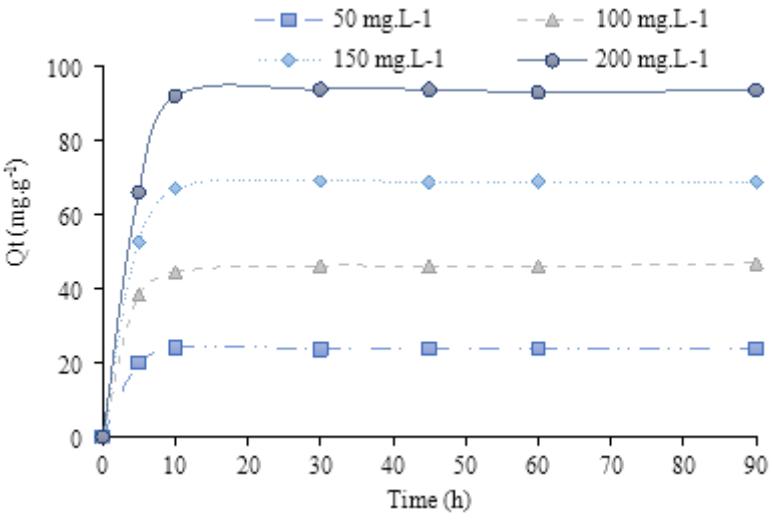

Figure 1

Kinetics of AR14 uptake by W. anomalus biomass at various initial dye concentrations

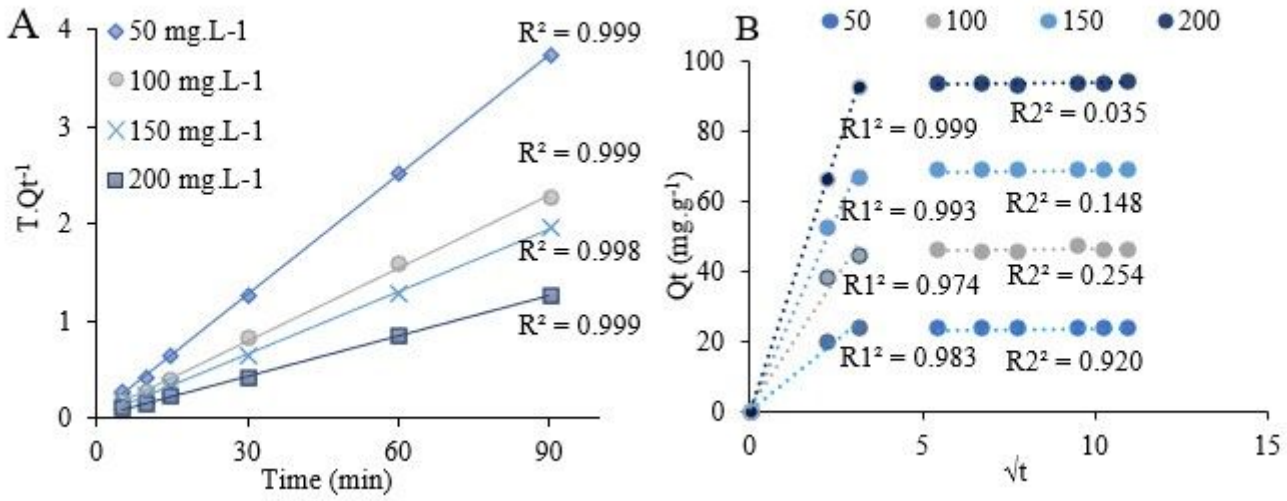

Figure 2

Plot of pseudo-second order model (A), and intra-particle diffusion model (B) of AR14 biosorption onto W. anomalus at various initial concentrations.

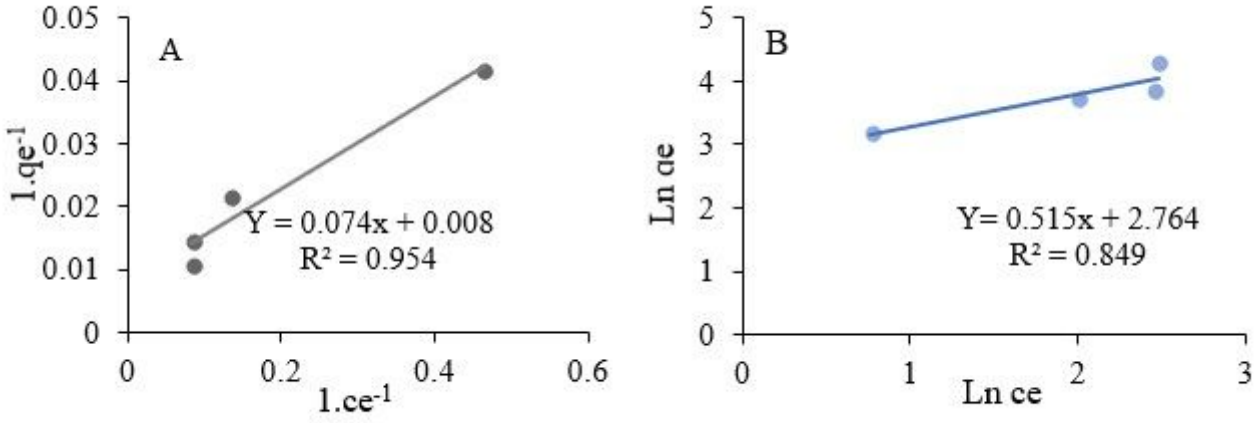

Figure 3

Langmuir (A) and Freundlich (B) isotherm plot and fitted models of AR14 biosorption by W. anomalus biomass

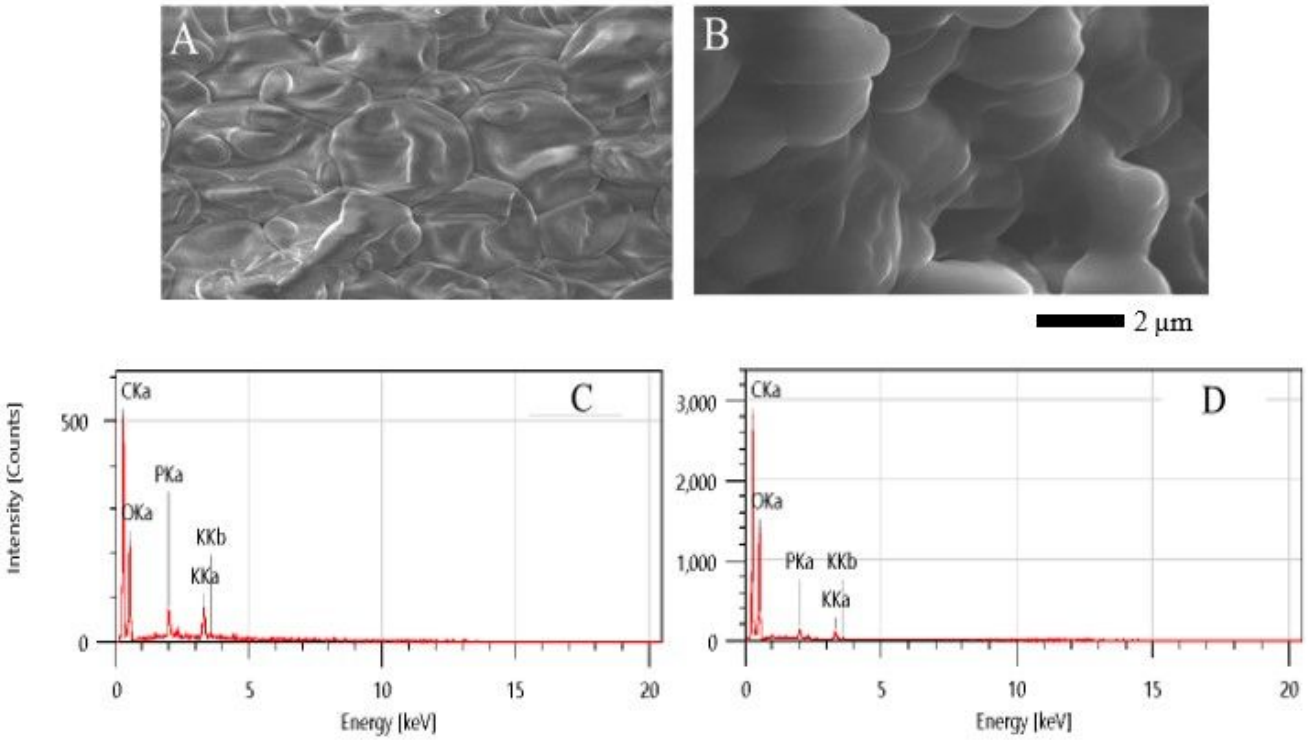

Figure 4

SEM of W. anomalus (x8000): (A) control yeast cells; (B) dye loaded cells at initial concentration 50 mg L-1, and the selected X-ray spectra of control (C) and dye loaded cells (D)

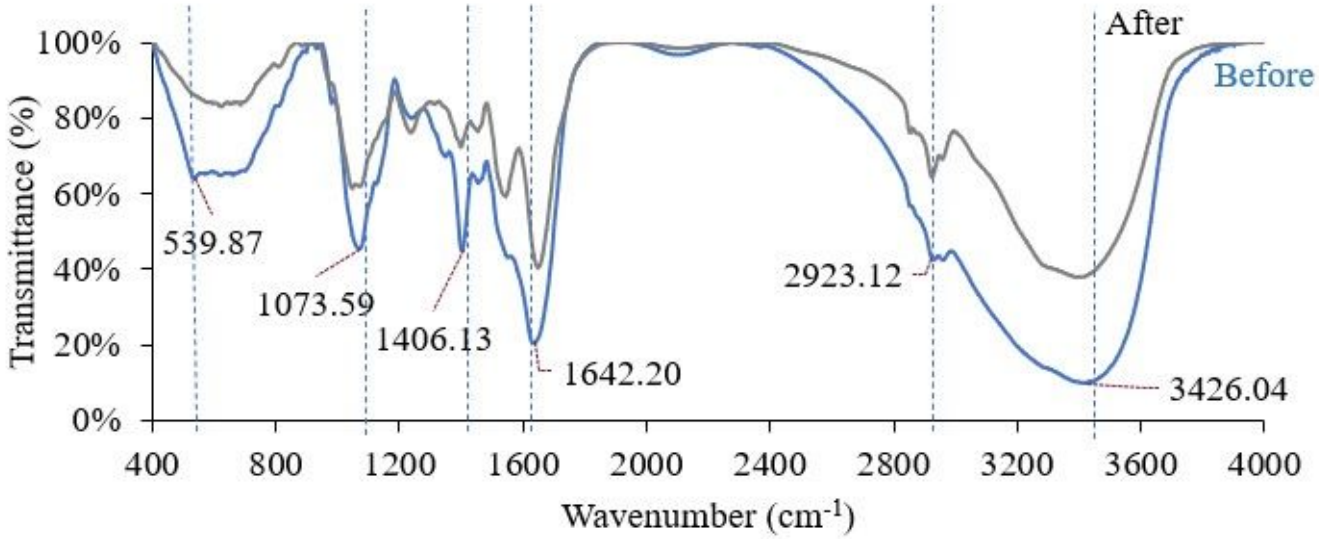

Figure 5

FTIR spectra of W. anomalus cells before and after AR14 biosorption

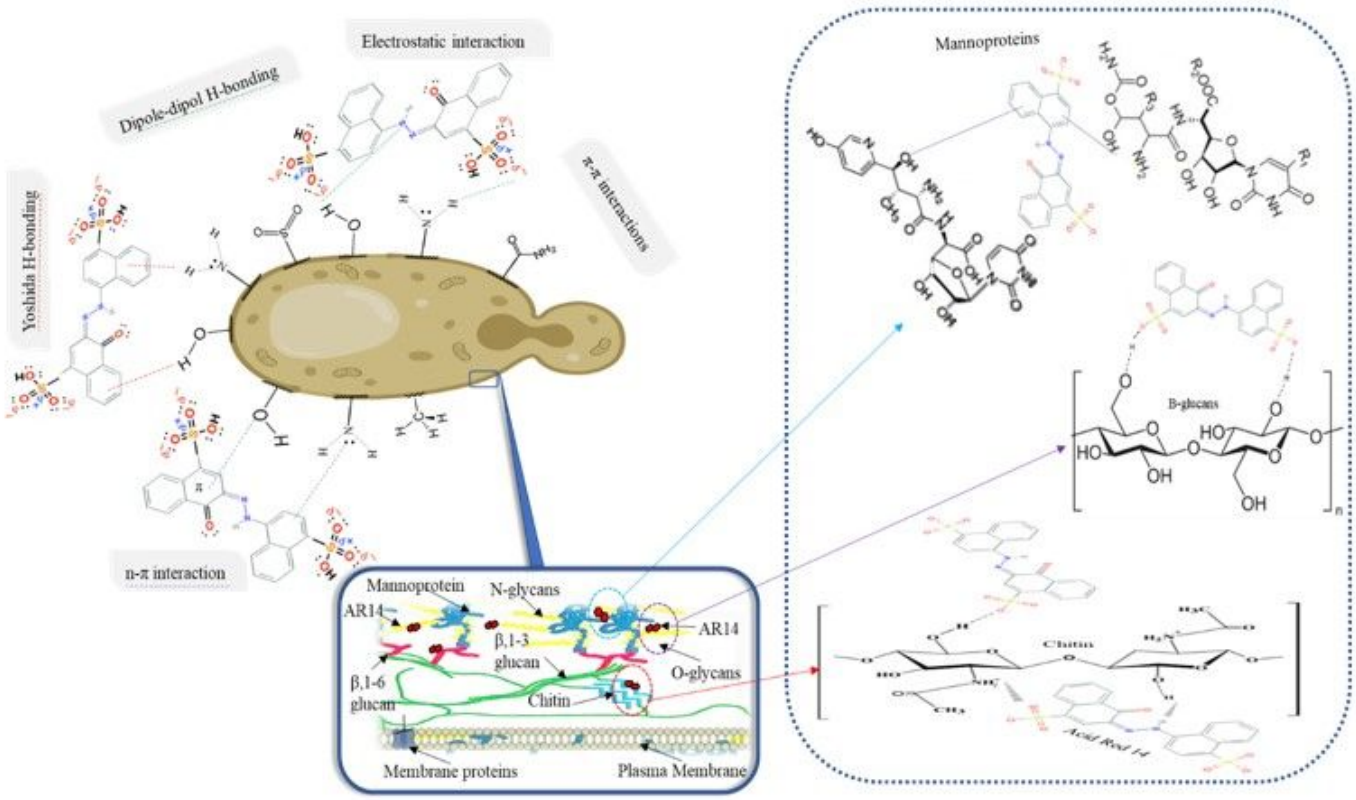

Figure 6

Architecture of yeast cell wall and proposed interaction mechanisms of AR14 biosorption

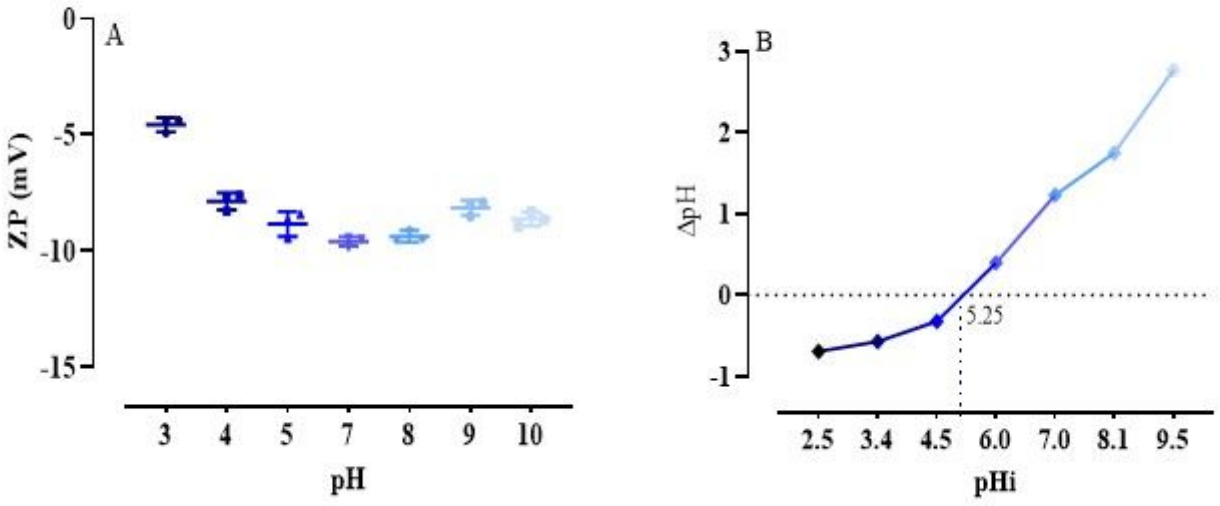

Figure 7

Zeta potential of (A) and pH zero charge (B) of W. anomalus yeast cells

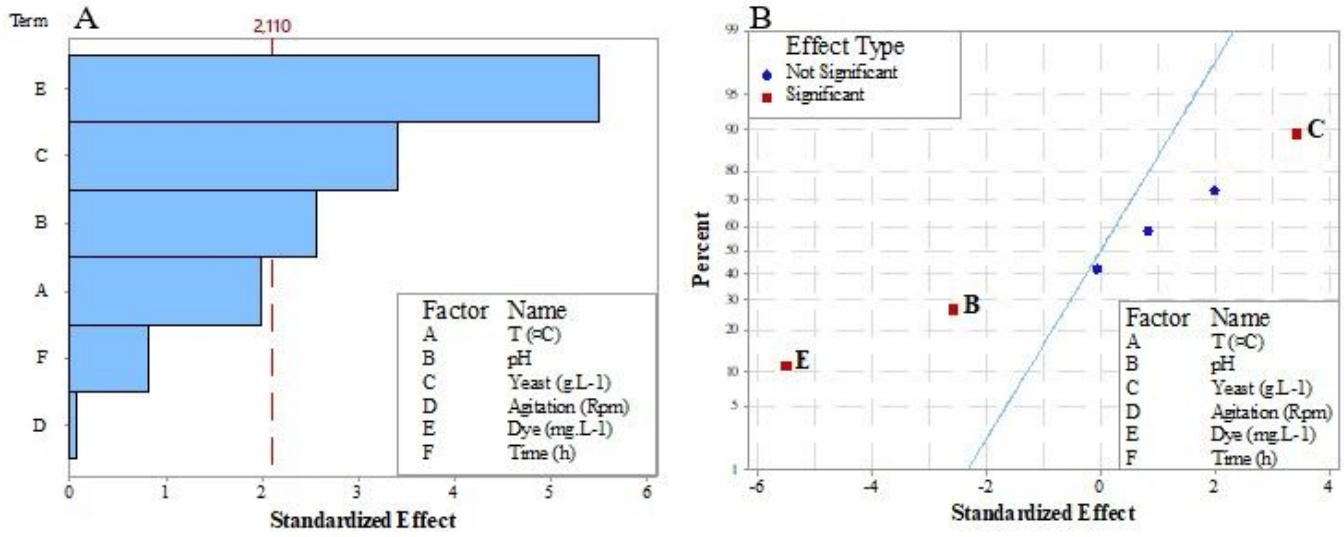

Figure 8

Main effect of variables on the biosorption capacity of AR14 using W. anomalus: Pareto chart of standard effect (A), and normal plot of standardized effects (B).

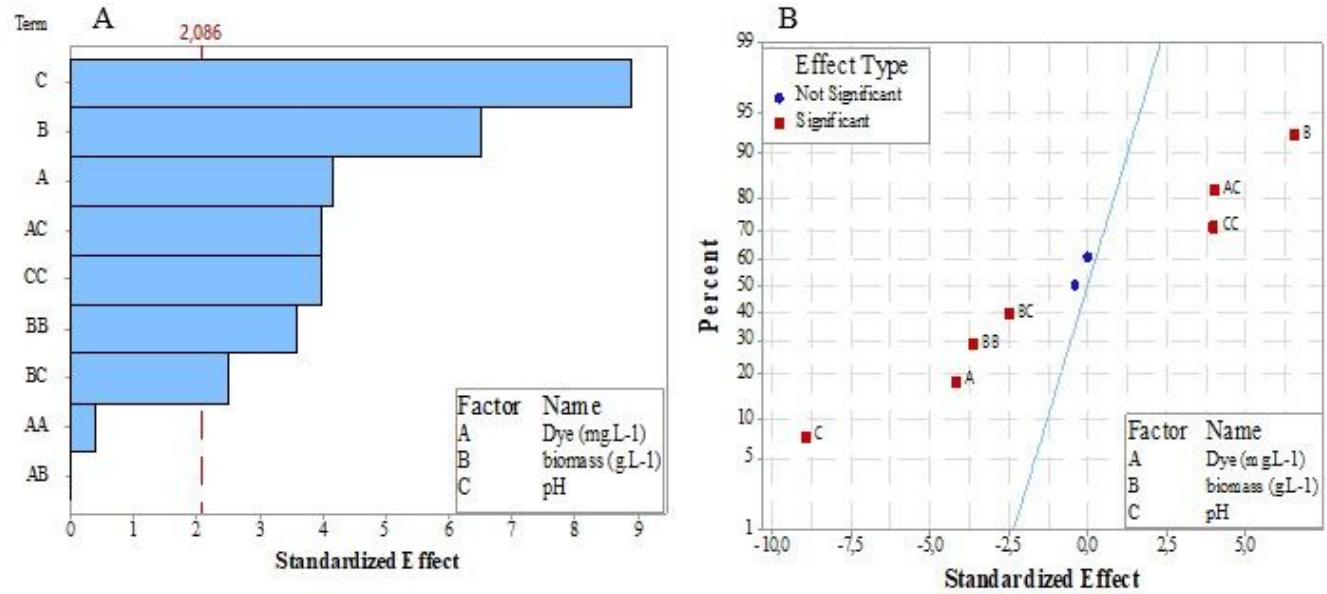

Figure 9

Effect of variables and 2-Way interaction on the biosorption capacity of AR14 using W. anomalus: pareto-chart of standardized effects (A), and normal plot of standardized effects (B).

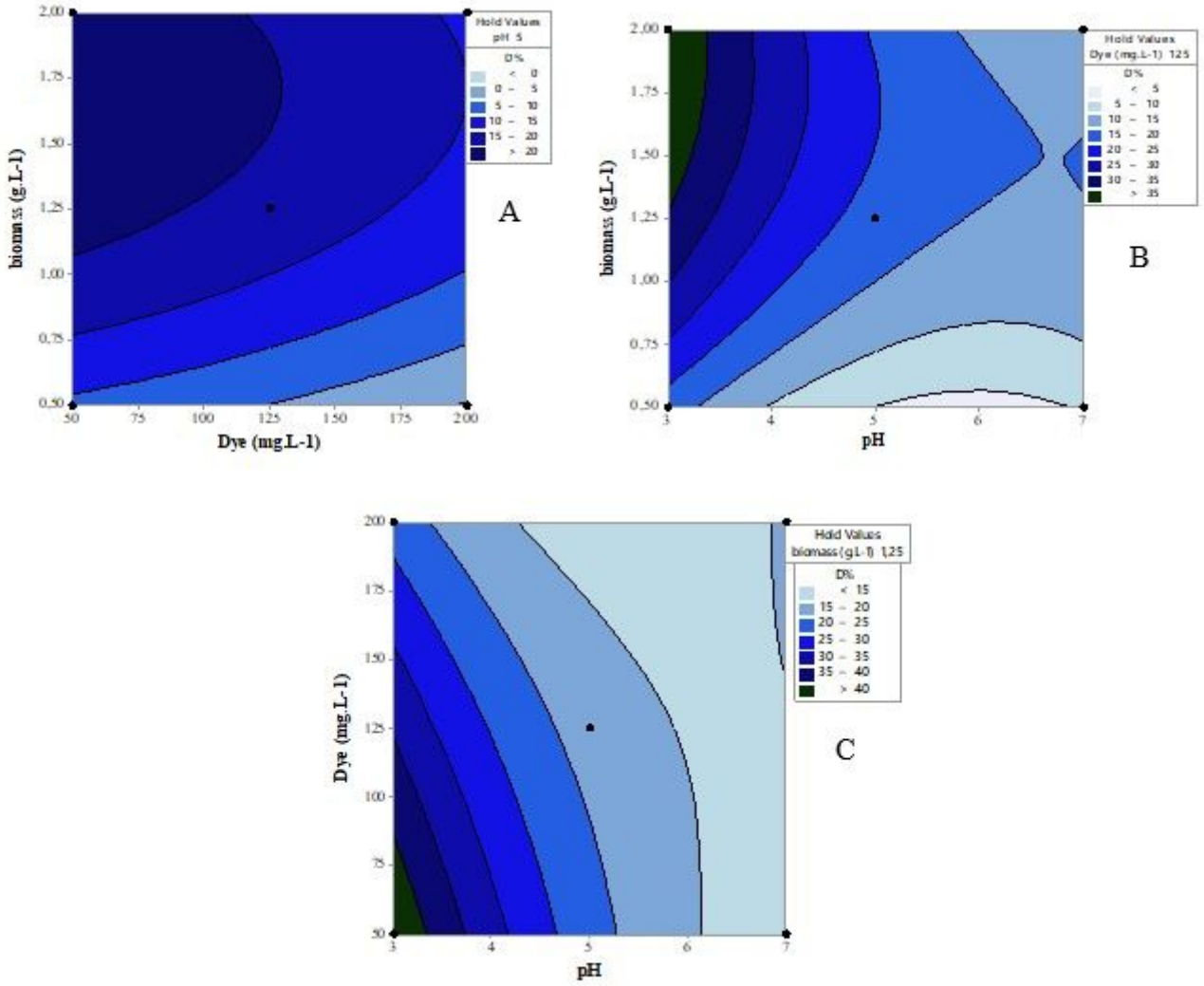

Figure 10

Effect of selected factors (pH, dye concentration and yeast biomass) on the biosorption capacity of AR14 onto W. anomalus.

Supplementary Files

This is a list of supplementary files associated with this preprint. Click to download.

- SupplementaryMaterial.docx